Stationary Frame Fault-Tolerant Current Control of Polyphase Permanent-Magnet Machines Under Open-Circuit and Short-Circuit Faults

Bhaskar Sen, *Student Member, IEEE*, and Jiabin Wang, *Senior Member, IEEE*

***Abstract*—The paper presents a stationary frame control strategy to achieve optimal current control for star-connected polyphase permanent-magnet machine under asymmetric phase faults, namely, phase open circuit (OC) and phase short-circuit (SC) condition. Current regulation under these faults is particularly challenging because optimal torque control strategy generates nonsinusoidal current references with unbalance in both fundamental and higher order working harmonics, to achieve minimal copper losses and torque ripple under fault condition. Under field-weakening operation, voltage limit introduces additional control problems. The paper describes a solution for these control issues by employing a novel controller in stationary frame. This control strategy allows minimal reconfiguration of the control structure from healthy to postfault operation. Extensive simulation and experimental results are presented as validation for the proposed strategy.**

***Index Terms*—Current control, fault tolerance, flux weakening, permanent-magnet machines, torque control, variable-speed drives.**

NOMENCLATURE

$V_{\rm dc}$	DC link voltage (V).
R	Phase resistance of the motor (Ω).
p	Number of pole-pairs.
L	Phase inductance of the motor (H).
i_j	Current in phase j (A).
ψ_j	Total flux linkage of phase j (V·s).
Ψ_{m1}, Ψ_{m3}	Fundamental and third harmonic flux linkage magnitude (V·s).
θ	Rotor angle in electrical radians (rad).
f	Electrical frequency (Hz).
k	Field weakening factor.
T_j	Torque contribution by phase j (N·m).
T_d	Demand torque (N·m).
T_f	Torque due to SC fault (N·m).
F_j	Fault index of phase *j*.
s	Laplace operator ($\rm s^{-1}$).
z^{-1}	Unit-delay operator.
λ_1, λ_2	Lagrange multipliers.
ω_{zn}, ξ_{zn}	Resonant angular frequency ($\rm rad.s^{-1}$) and damping factor of the *n*th complex zero.
ω_{pn}	Resonant angular frequency of the *n*th complex pole ($\rm rad.s^{-1}$).
k_∞	Proportional gain.
ZOH	Zero-order hold.

Manuscript received May 22, 2015; revised August 3, 2015; accepted August 31, 2015. Date of publication September 11, 2015; date of current version January 28, 2016. This work was supported in part by the European ENIAC Joint Undertaking under the MotorBrain project. Recommended for publication by Associate Editor J. Hur.

The authors are with the Electrical Machines and Drives Research Group, Department of Electronic and Electrical Engineering, The University of Sheffield, Sheffield, S1 3JD, U.K. (e-mail: elp11bs@sheffield.ac.uk; j.b.wang@sheffield.ac.uk).

Color versions of one or more of the figures in this paper are available online at http://ieeexplore.ieee.org.

Digital Object Identifier 10.1109/TPEL.2015.2478337

I. INTRODUCTION

FAULT-TOLERANT operations are increasingly becoming important in improving reliability and safety of electric drives, especially in aerospace and automotive sectors [1], [2]. Operation under fault condition commonly known as "limp-home" mode [3] is essential for providing high degree of availability, and reliability demanded in safety critical application such as flight control surface actuation and electric vehicle traction. To improve fault handling capability further, multiphase machines have been proposed in [1] and [4] due to more degrees of freedom available for postfault operation and control compared to three-phase machines.

The issues associated with fault-tolerant operation in permanent-magnet machines can be divided into two major tasks. The first task is to generate appropriate current references that produce minimum torque ripple and minimum copper losses under fault conditions. In [5]–[8], zero-torque ripple under open circuit (OC) fault was achieved by adjusting phase current angles to produce forward rotating stator magnetomotive force (MMF). However, this method is applicable when rotor flux is purely sinusoidal and does not lead to minimum copper loss. The performance deteriorates further in practical PM machines that have higher order harmonics in back-EMF [9]. In [10]–[13], current references was optimized for maximum torque based on off-line calculations accounting for third harmonic in back-EMF for a five-phase machine with different winding configurations under OC fault. In [14]–[18], an online optimal current reference generation technique was presented for phase short-circuit (SC) and OC faults, which minimized the overall stator copper losses. However, operation under field weakening mode was not addressed. Optimal torque control (OTC) proposed in [19] obtained minimum stator copper loss with online computation of the current references under both OC and SC faults. Furthermore, with application of a weighting factor on the flux linkage, the OTC could be used in field-weakening regime. However, this method was only applied to five-phase machine with each phase driven individually by H-bridge converters. Modifying the current references such that OTC can be applied to star-connected

machines can extend the applicability of the technique to a larger class of machines.

The second task is the tracking control of the generated current references. Tracking the current references obtained through the OTC or other current reference generation techniques is quite challenging. This is because under fault conditions, the machine loses its symmetry and the standard synchronous frame based current control is no longer effective due to presence of time-varying components. This is particularly problematic in the OTC since the current references generated by the OTC algorithm are typically unbalanced and have higher order harmonics [19]. Hysteresis current controller is typically employed for current controls [5]–[8], [11], [12], [14]–[16], [19]. However, this results in variable switching frequency, which increases switching loss and electromagnetic interference (EMI) emission. In [20] and [21], a synchronous frame current control technique based on modified Clarke transformation was proposed for pulsewidth modulated (PWM) drives under OC fault. However, higher order harmonics in back-EMF was ignored in torque computation and operation under phase SC fault, field weakening as well as transition of control from healthy to fault were not addressed. In [22], postfault control of six-phase induction machine was presented for low-speed operation using additional negative sequence controllers under OC fault operation. In the various control methods proposed in literature, a general control technique for tracking current references, which are unbalanced and contains higher order harmonics under inverter voltage limit has not been addressed.

One solution to tracking time-varying signals is proportional–resonant (PR) controllers [23]–[25], which have been employed for applications in active harmonic filtering in grid applications. However, they are optimized to operate around a fixed fundamental frequency since the grid fundamental frequency varies only slightly. In variable-speed drives, however, the fundamental frequency of motor currents is speed dependent. Analysis of transient response of resonant controller for variable-speed drive application was performed in [26] only for a narrow range of frequency (30–50Hz). However, fundamental frequency varies over a wide range especially in multipole PM drives. In addition, the standard PR controllers are not suitable for operation near the inverter modulation limit due to their inherently high open loop gain, which may cause stability problem under voltage saturation [27]. To improve performance under voltage saturation, an antiwindup scheme was proposed in [27] for the PR controller, albeit operation under only single excitation frequency was demonstrated. In [28], an alternative control strategy was proposed to solve the antiwindup problem for operation under fixed fundamental frequency.

This paper is concerned with control of a fault-tolerant PM machine under OC or SC fault with a unified control strategy, which allows for smooth transition between healthy and fault modes of operation. The paper contributes to the body of knowledge in the following aspects:

1) extension of the OTC reference generation for star-connected PM machine;
2) a new stationary frame resonant current controller structure operating with fixed PWM switching frequency, it is capable of tracking time-varying current references with multiple frequency components, which vary with drive speed, and operate stably under controller output voltage saturation;
3) voltage injection technique under fault condition to increase modulation range and dc-link voltage utilization in conjunction with the proposed resonant control;
4) field-weakening algorithm based on a search algorithm for operation under healthy and fault operation in conjunction with the proposed resonant control.

The rest of the paper is organized as follows. Section II describes optimal current reference generation for star-connected PM drives operating under healthy or fault mode in both constant torque and field weakening regions. Section III develops resonant current control for tracking the time-varying references in stationary frame over a wide speed range with due account of voltage saturation. Section IV presents a zero voltage injection scheme to extend drive operating range, and Section V addresses the issue pertinent to field weakening operation. Experimental results are presented and discussed in Section VI before conclusion is given in Section VII.

II. Optimal Current Reference Generation

In order to obtain optimal currents under fault conditions, the demand torque should be met and the ohmic losses should be minimized [29]. This is because windings are limited in their heat dissipation capacity and injecting more current to obtain prefault torque level will lead to overheating of the winding, possibly leading to further failure. However, minimizing ohmic losses does not result in optimal currents during field weakening operation, since the inverter output voltage is limited by the dc-link voltage and the drive will not be able to realize the reference currents due to control saturation. Hence, a cost function that minimizes both currents and voltages is needed. This can be achieved using the OTC, wherein for a given torque demand T_d, the phase current references of an *m*-phase SPM machine can be obtained by minimizing a cost function given by

$$\Lambda = \sum_{j=1}^{m} (Li_j + kF_j\psi_j)^2. \tag{1}$$

The fault index F_j is defined as

$$F_j = \begin{cases} 1, & j \neq l \\ 0, & j = l \end{cases} \tag{2}$$

where *l* is the faulted phase. The flux linkage ψ_j and the instantaneous torque T_j of *j*th phase can be expressed as

$$\begin{aligned} \psi_j =\ & \Psi_{m1}\cos\left[\theta-(j-1)\,2\pi/m\right] \\ & +\Psi_{m3}\cos\left\{3\left[\theta-(j-1)\,2\pi/m\right]\right\} \\ T_j =\ & a_j(\theta)\,i_j = p\left(\frac{d\psi_j}{d\theta}\right)i_j \end{aligned} \tag{3}$$

where p is the number of pole pairs. The currents references have to meet the torque demand constraint given as

$$T_d = \sum_{j=1}^{m} F_j a_j(\theta)\,i_j. \tag{4}$$

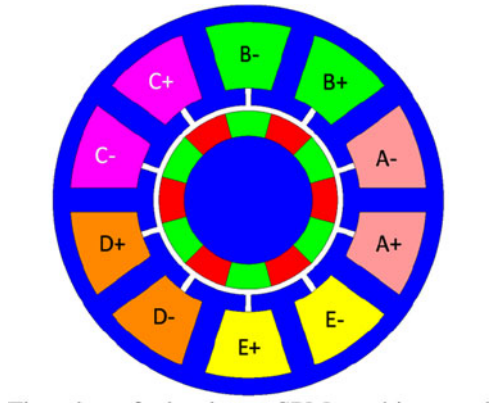

Fig. 1. Five-phase fault-tolerant SPM machine topology.

For the case of a short-circuit fault in phase l, the pulsating torque T_f, given by (5) generated by the SC current i_l, should be cancelled by the torque produced by the remaining phases in order to obtain zero torque ripple

$$T_f = \begin{cases} 0, & \text{OC fault} \\ a_l(\theta)\, i_l, & \text{SC fault} \end{cases}. \tag{5}$$

Since the phase windings of the fault-tolerant machine considered are star-connected, Kirchhoff current law for the healthy phases given by (6) needs to be considered in the overall minimization, i.e.,

$$0 = \sum_{j=1}^{m} i_j F_j. \tag{6}$$

The objective function of the constrained optimization problem can be obtained by applying the method of Lagrange multipliers expressed by

$$\Lambda = \sum_{j=1}^{m} \left(L i_j + k F_j \psi_j\right)^2 + \lambda_1 \left[T_d - T_f - \sum_{j=1}^{m} \left(F_j a_j(\theta)\, i_j\right)\right] + \lambda_2 \sum_{j=1}^{m} i_j F_j. \tag{7}$$

The instantaneous current in phase j can then be derived by minimizing the objective function and is given by (8)–(9), and 10 shown at the bottom of the page

$$i_j = \frac{-\lambda_2 F_j + \lambda_1 F_j a_j - 2k F_j \psi_j L}{2L^2} \tag{8}$$

$$\lambda_2 = \frac{\left(\lambda_1 \sum_{j=1}^{m} F_j a_j - 2kL \sum_{j=1}^{m} F_j \psi_j\right)}{\sum_{j=1}^{m} F_j} \tag{9}$$

TABLE I
SPECIFICATION OF THE PROTOTYPE FIVE-PHASE FAULT-TOLERANT PM MACHINE

Maximum speed	3000 r/min	Phase resistance	380 mΩ
Rated torque	1.86 N·m	Phase inductance	2.8 mH
Rated rms	$6.5/\sqrt{2}A$	Cable Resistance/phase	300 mΩ
Number of phases	5	DC link voltage	50 V
Number of pole pairs	6	Fundamental flux linkage magnitude (Ψ_{m1})	19.1 mV·s
Switching/Sampling frequency	10 kHz	Third harmonic flux linkage magnitude (Ψ_{m3})	416 μV·s

For the purpose of simulation and experimental validation a five-phase fault-tolerant PM machine shown in Fig. 1 is considered, and its specification and parameters are given in Table I. It is to be noted that this machine topology has negligible mutual inductance between phases [30].

It should be noted that the proposed reference current generation is an extension of the technique described in [19] for separately excited phase windings to the star-connected winding configuration. It yields smooth torque under healthy and fault conditions with minimum copper loss while satisfying voltage constraint at high speeds. The proposed method, and those presented in [14]–[18] has lower joule loss per unit torque for star-connected machines compared to the offline methods [10]–[13]. However, the methods presented in [10]–[18] cannot operate under field weakening.

Fig. 2 shows the current references and their spectrums generated from the optimal current control technique with $T_d = 0.7$ N·m, and $k = 0.7$ when phase 1 (i.e., phase A) is open circuited. It can be clearly seen that the currents have the first, third, and fifth harmonics although the fifth harmonic is quite small. This is expected since back-EMF of the machine contains only the first and third harmonic components, the interaction of the same frequency components contribute to average torque. By minimizing the ohmic losses, even-order harmonics will not be present since it does not contribute to average torque. It can also be seen from the FFT plots that the fundamental and third harmonic components in each phase are different. Current references for a phase SC fault can be similarly generated, and they exhibit the similar features to those of the OC fault. Due to space limitations, the SC results are not shown. The presence of the high-order harmonics and unbalance poses a challenging problem for current reference tracking. This issue will be addressed by control design elaborated in the next section.

III. CURRENT CONTROL

Traditionally current control in PM drives is performed in synchronous reference frame [31], in order to convert sinusoidal

$$\lambda_1 = \frac{\left\{2L^2\left(T_d - T_f\right)\sum_{j=1}^{m} F_j + 2kL\left[\begin{array}{l}\sum_{j=1}^{m} F_j\left(\sum_{j=1}^{m} F_j a_j \psi_j\right) \\ -\sum_{j=1}^{m} F_j \psi_j\left(\sum_{j=1}^{m} F_j a_j\right)\end{array}\right]\right\}}{\left[\sum_{j=1}^{m} F_j\left(\sum_{j=1}^{m} F_j a_j^2\right) - \left(\sum_{j=1}^{m} F_j a_j\right)^2\right]} \tag{10}$$

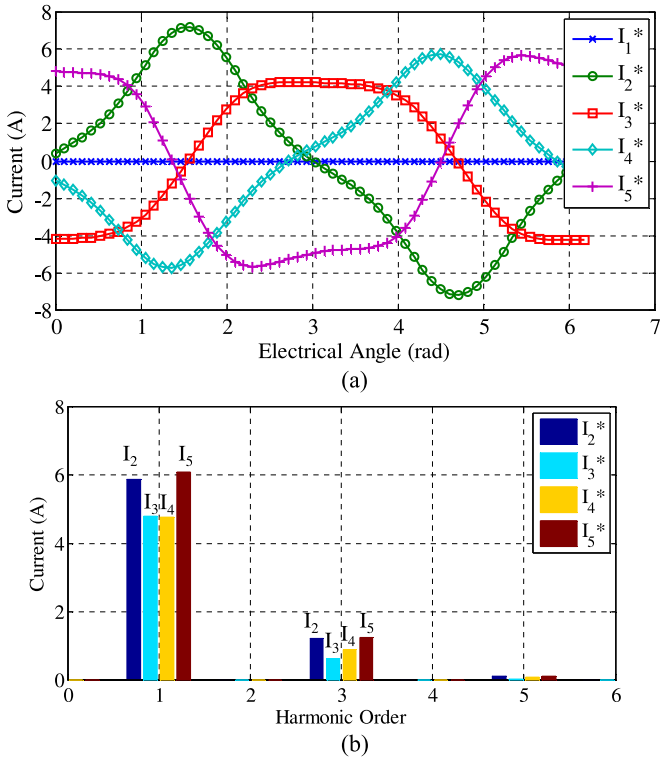

Fig. 2. OTC with OC fault in phase 1 with $T_d = 0.7$ N·m and $k = 0.7$: (a) instantaneous currents and (b) FFT.

current references, which are time-varying into direct current (DC) references. This control structure is effective only if a machine operates in symmetrical or balanced conditions. However, the balanced condition is no longer true when a fault occurs. Although many authors have proposed modified control structure in synchronous reference in order to maintain operation under fault condition [20]–[22], [32], most of the methods are focused on the OC fault, assuming current and back-EMF to be single frequency and operating in the constant torque region.

To track the reference currents generated by the OTC, current control in the natural stationary frame (*abcde*) is proposed. The benefit of the tracking control in the natural stationary frame is that the controller structure remains same in healthy and fault conditions, except for turning off the controls for a faulted phase. In doing so, the controllers in the other healthy phases are not affected. Secondly, under field weakening operation, voltage saturation can be dealt with individually for each phase rather than combined in the form of space vectors. However, the drawback of this method is that the control references are no longer constant quantities but is time-varying with higher order harmonics, which make the controller design more challenging.

One of the effective methods for tracking periodic time-varying currents in stationary reference frame is PR control and its variants [23]–[25], [33]. For tracking multiple frequency references, a number of resonant controllers are usually employed in parallel. Since the resonant poles are located at frequencies of interest, steady state tracking is guaranteed. However, one of the limitations of the PR control is that the location of its open-loop zeroes is not placed directly. This can be appreciated as follows

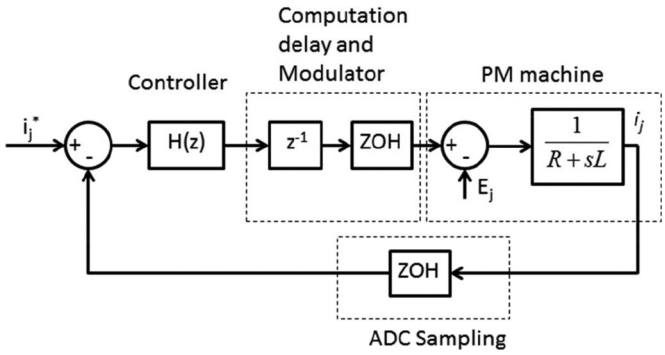

Fig. 3. Proposed current controller structure.

using an example of single PR controller:

$$H(s) = K_p + K_{I1}\frac{s}{s^2+\omega_1^2} = K_p\frac{s^2+2\left[K_{I1}/(2\omega_1 K_p)\right]\omega_1 s+\omega_1^2}{s^2+\omega_1^2}. \quad (11)$$

It can be seen that the order of the numerator is the same as that of the denominator. However, there is only one degree of freedom (damping coefficient), which can be specified by gain selection for K_p and K_{I1}, whereas the natural resonant angular frequency in the numerator has to equal the angular frequency ω_1 of the tracking reference. Moreover, the location of the zeroes can change as more resonant controllers are added in parallel to track references with more than one frequency components. It is well known that open-loop zeroes affect the transient performance [34]; therefore, although the above structure will enable zero steady state tracking error, the control system performance may be limited by the inability to place the zeroes optimally [28].

The restriction on open-loop zeroes can be solved by employing an alternate control law given as follows:

$$H(s) = K_\infty \prod_{n=1,3,\ldots,n} \frac{s^2+2\xi_n\omega_{\rm zn}s+\omega_{\rm zn}^2}{s^2+\omega_{\rm pn}^2} \quad (12)$$

where $\omega_{\rm zn}$ and $\xi_{\rm zn}$ are the resonant angular frequency and the damping factor of the *n*th complex zero, respectively, and ω_{pn} is the resonant angular frequency of the *n*th complex pole, corresponding to the desired frequency component(s) to be tracked by the controller. This controller enables independent selection of the locations of its resonant poles and zeroes.

In addition, resonant controllers are sensitive to discretization when transforming from *s*-domain to *z*-domain for real-time implementation [35]. It is therefore preferable to design the controller in *z*-domain, to avoid performance deterioration introduced by discretization [28]. The control law given by (12) can be discretized using matched *z* transformation to maintain the location of poles and zeroes. The resonant controllers can have stability problem when the delay introduced by digital sampling is significant with respect to the fundamental frequency [35], [36]. In order ensure control stability at high fundamental frequencies, a predictive compensation technique is used [28], resulting in the final controller structure given by (13) and (14)

TABLE II
OPTIMIZED CONTROLLER PARAMETERS

Parameter	Value	Parameter	Value
K_∞	16.00	ω_{z3c}	−14.84
ω_{z1c}	21.311	$k_{z3\omega}$	14.42
$k_{z1\omega}$	2.835	ξ_{3c}	0
ξ_{1c}	0.9633	$k_{3\xi}$	0
$k_{1\xi}$	−3.2e-3	p_{1c}	0.72
		k_{p_1}	6.02e–4

and shown in Fig. 3

$$H(z) = K_\infty \frac{z}{z+p_1} \prod_{n=1,3,\ldots,n} \frac{z^2 - a_{1n} z + a_{2n}}{z^2 - 2z\cos\omega_{pn} T_s + 1} \quad (13)$$

$$\begin{aligned} a_{1n} &= 2e^{\sigma}\cos(\upsilon_{\mathrm{zn}} T_s) \\ a_{2n} &= e^{2\sigma} \\ \sigma &= -\xi_n \omega_{\mathrm{zn}} T_s \\ \upsilon &= \omega_{\mathrm{zn}}\sqrt{1-\xi_n^2} \end{aligned} \quad (14)$$

where a_{1n} and a_{2n} are the controller coefficients corresponding to the *n*th complex zero and T_s is the sampling time, assumed to be 100 μs in this study. Further, n is limited to 3, in this study, implying only the first and third harmonics of the current reference are actively controlled.

Due to speed, hence frequency variations, it is necessary to tune the controller over a wide operating speed range. This is particularly challenging since it implies that, as the resonant poles move with operating speed of the machine, the closed-loop poles and zeroes and the open-loop resonant poles of the system will move with the system frequencies. Therefore, the open-loop zeroes have to be modified as a function of system frequencies in order to achieve acceptable control performance.

For the five-phase machine illustrated in Section II, at least two current harmonics, namely, the fundamental and the third harmonic needs to be controlled. In order to keep the complexity of the controls to minimum, the poles and zeroes of the system are scaled as a linear function with respect to the system fundamental electrical frequency *f* expressed as

$$\begin{aligned} \omega_{p1} &= 2\pi f, \quad \omega_{p3} = 3\times 2\pi f \\ \omega_{z1} &= \omega_{z1c} + k_{z1\omega} f \\ \xi_1 &= \xi_{1c} + k_{1\xi} f \\ \omega_{z3} &= \omega_{z3c} + k_{z3\omega} f \\ \xi_3 &= \xi_{3c} + k_{3\xi} f \\ p_1 &= p_{1c} + k_{p1} f \end{aligned} \quad (15)$$

where (ω_{z1c}, $k_{z1\omega}$) and (ω_{z3c}, $k_{z3\omega}$) are the constant intercepts and frequency-scaling coefficients of the resonant angular frequencies of the complex zeroes (ω_{z1}, ω_{z3}), respectively. (ξ_{1c}, $k_{1\xi}$) and (ξ_{3c}, $k_{3\xi}$) are the constants and frequency-scaling coefficients for the damping factor of the first and the third complex zero, respectively. (p_{1c}, k_{p_1}) are the constant and frequency-scaling coefficients for the real pole p_1. The 11 tunable parameters of the system are selected through an optimization process to minimize the integral-square error (ISE) given as follows [37]:

$$C = \sum_f \int (y(t) - u(t))^2 dt \quad (16)$$

where *y*(*t*) and *u*(*t*) denote, respectively, the output and the input (reference) of the closed-loop system at system frequency *f*. The objective function *C* is the sum of the ISE errors over the target system frequency range [30–300 Hz], corresponding to speed range of [300–3000 r/min]. Operation below 30 Hz can simply be achieved using only proportional gain since the

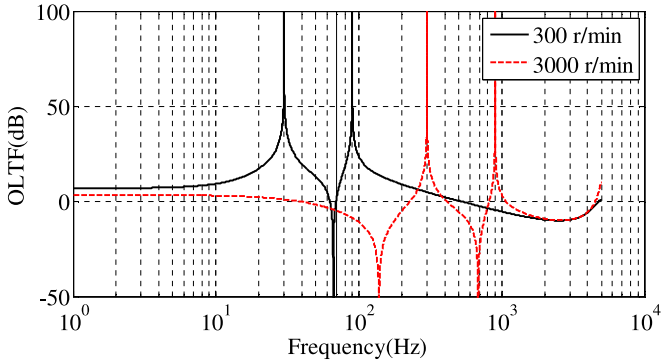

Fig. 4. Open-loop transfer function magnitude plots at 300 and 3000 r/min.

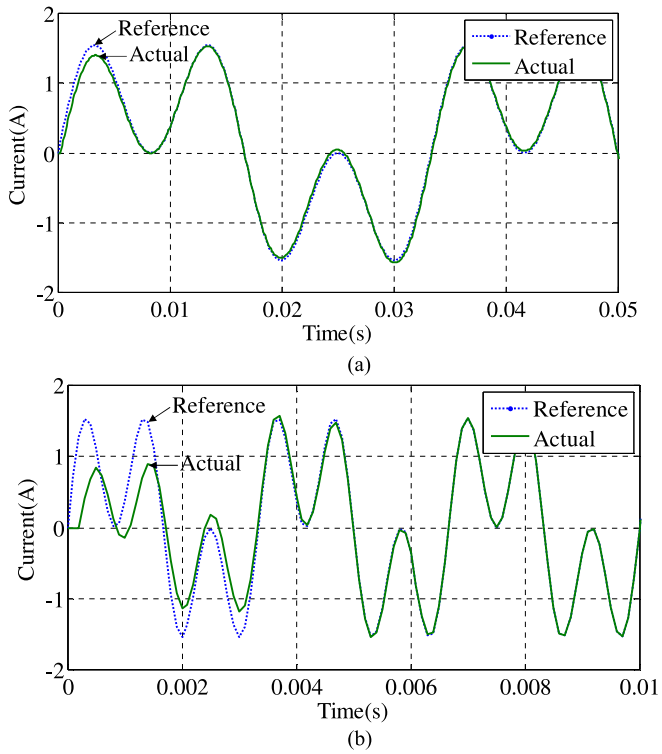

Fig. 5. Tracking performance of proposed resonant controller at (a) 300 r/min and (b) 3000 r/min. (Dot) Reference current and (solid) closed-loop current response.

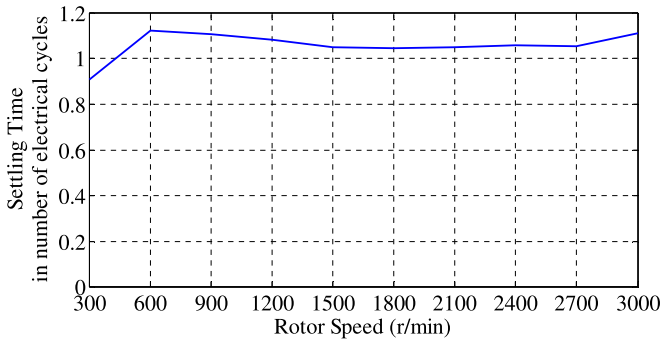

Fig. 6. Settling time variation in number of electrical cycles (+/− 4% criterion) with motor speed.

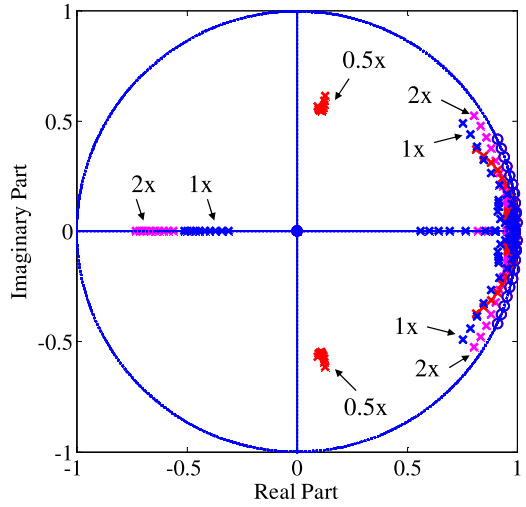

Fig. 7. Movement of closed-loop poles (x) and zeros (o) under (0.5x, 1x and 2x) variation of motor phase resistance and inductance. 1x is nominal parameters.

bandwidth will be sufficient to obtain desirable current tracking. The optimization is performed using *patternsearch* function in the global optimization toolbox in MATLAB [38].

Some constraints need to be imposed during optimization in order to reduce computation time and avoid searching unfeasible controller parameters. Since the controller is not actively tracking the fifth harmonic while the OTC algorithm does generate a small fifth harmonic in the reference, the closed-loop transfer function should have a gain of 0 dB or less at the fifth harmonic frequency to ensure that the fifth harmonic will not be amplified under healthy conditions, and it can be expressed as

$$20\log\left(|\mathrm{CLTF}|_{\omega=5\omega_e}\right) \leq 0. \tag{17}$$

The closed-loop transfer function should have a low peak gain such that in events of speed change, the delay in speed measurement will not lead to excessive overshoots. This condition can be expressed as

$$\max\left(20\log\left(|\mathrm{CLTF}|\right)\right) \leq 1.8. \tag{18}$$

The maximum value of controller proportional gain is a tradeoff between transient response and noise sensitivity and is

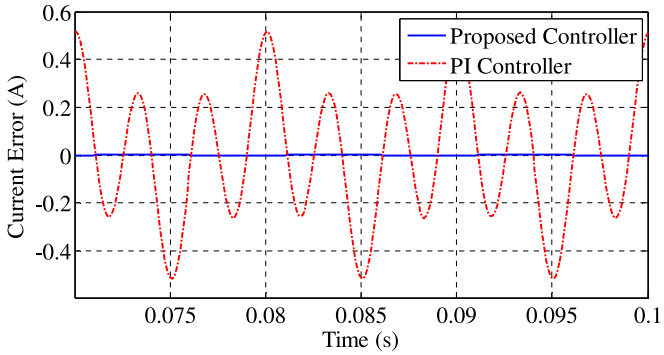

Fig. 8. Current error comparison of the proposed controller with PI controller with same control bandwidth (1 kHz) at 1000 r/min.

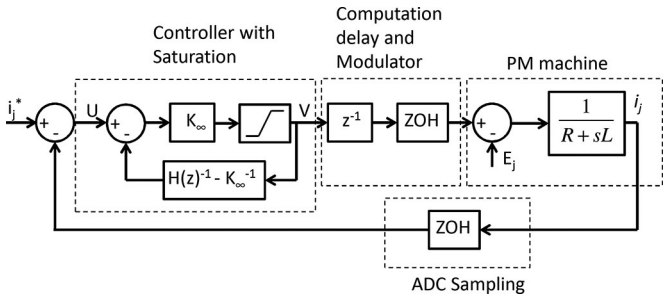

Fig. 9. Controller structure with antiwindup.

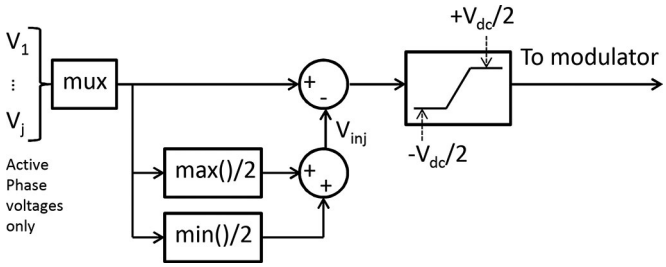

Fig. 10. Zero-sequence voltage injection.

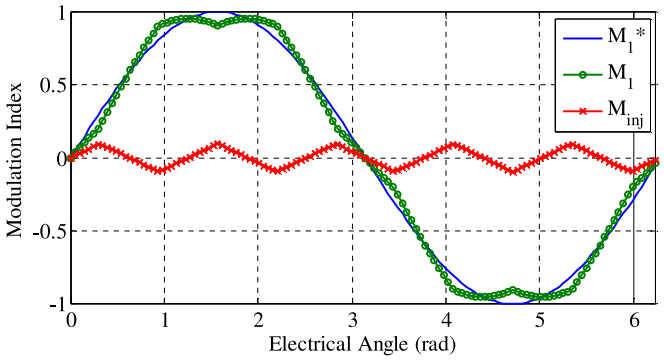

Fig. 11. Modulation index with and without voltage injection (only phase 1 is shown).

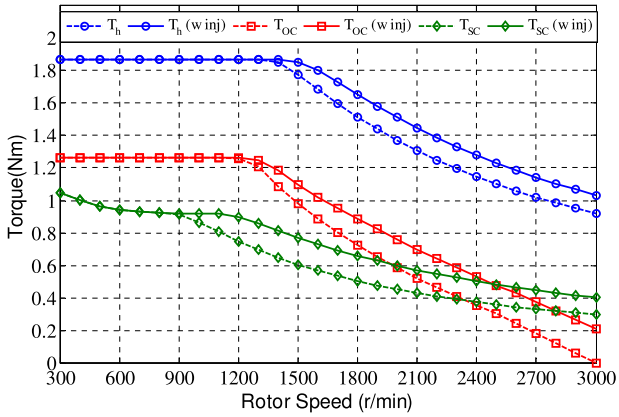

Fig. 12. Torque–speed characteristic under healthy (h), single-phase OC and single-phase SC (SC) with (w inj) and without voltage injection.

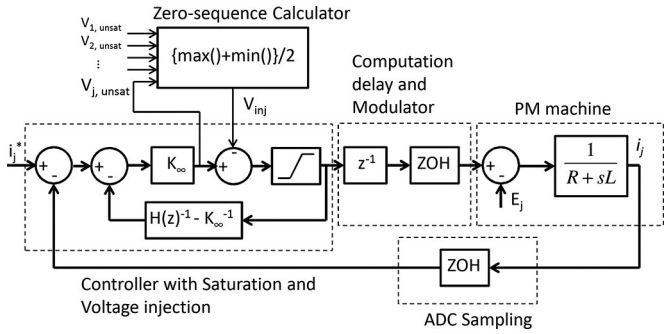

Fig. 13. Final controller structure including voltage injection.

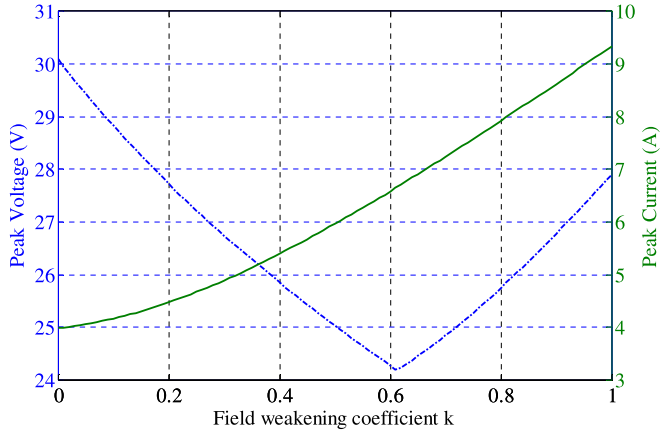

Fig. 14. Effect of field weakening coefficient k on voltage and current ($T_d = 0.71$ N·m at 2000 r/min). (Dashed-dotted) Peak voltage (V) and (solid) peak current (A).

limited to 16 in order to limit the open-loop bandwidth to about $f_s/10$. To constrain the optimization search, the maximum frequency of zeroes is restricted to six times the system angular frequency. The search constraints for parameters are given in (19), and the results of the optimal design are summarized in Table II

$$\begin{aligned} 1 &\le K_\infty \le 16 \\ -1 &\le p_1 \le 1 \\ 0.01\omega_e &\le \omega_{z1} \le 6\omega_e \\ 0 &\le \xi_1 \le 4 \\ 0.01\omega_e &\le \omega_{z3} \le 6\omega_e \\ 0 &\le \xi_3 \le 4. \end{aligned} \tag{19}$$

It can be observed from the optimized controller parameters that both $k_{3\xi}$ and ξ_{3c} is zero, and therefore, the damping ratio ξ_3 need not be computed online but simply set to 0. Fig. 4 shows the bode plot of the open-loop transfer function (OLTF) for two rotor speeds. It can be observed that for the plot associated with each speed, there are two resonant poles corresponding to the first and the third harmonics. In the lower speed regime only one zero with low damping corresponding to ω_{z3c} can be observed, whereas in the high-speed operation both zeroes exhibit low damping as expected from the damping factor frequency-scaling coefficients (ξ_{1c}, $k_{1\xi}$). It is worth mentioning that the developed current controller will also work with other methods of current reference generation.

Fig. 5 shows the controller tracking response at 300 and 3000 r/min. It can be observed that the controller is able to track the references within 1.2 electrical cycle. In order to quantify this further, theoretical settling time of the controller at various operating speeds of the machine is shown in Fig. 6. The average settling time of the controller is less than 1.2 electrical cycles. It should be pointed out that it is possible to tune resonant controller(s) for a fast settling time of less than a quarter cycle of a reference with fixed frequency as reported in [28]. However, this is not the case if the frequency of a reference varies unless the proportional gain is increased to a high value, which would compromise noise rejection property.

Fig. 7 shows the variations of closed-loop poles when the motor parameters are varied from 0.5 to 2 times their nominal values. It can be seen that although the poles/zeroes are shifted from those designed with the motor nominal parameters, they are within the unit circle and hence the system is robust even with four times variations in parameters.

Fig. 8 compares the current error of the proposed control verses a conventional PI controller with back-EMF feed-forward compensation for the same control bandwidth (1 kHz) at 1000 r/min with the same current reference as shown in Fig. 5. It can be seen that the PI controller results in a large current error while the resonant control gives superior performance as noted in previous literature [23]–[25], [33].

Resonant controllers due to its inherently high gain at the resonant angular frequency can quickly wind up when operating close to the voltage limit. An anti-winding-up protection similar to that reported in [28] and [34], shown in Fig. 9, is employed. It can be shown that under linear condition (no saturation), the closed-loop transfer function of the inner controller feedback

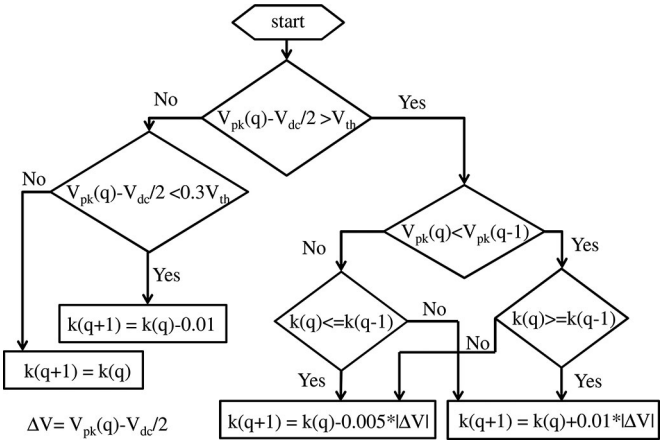

Fig. 15. Field-weakening flowchart.

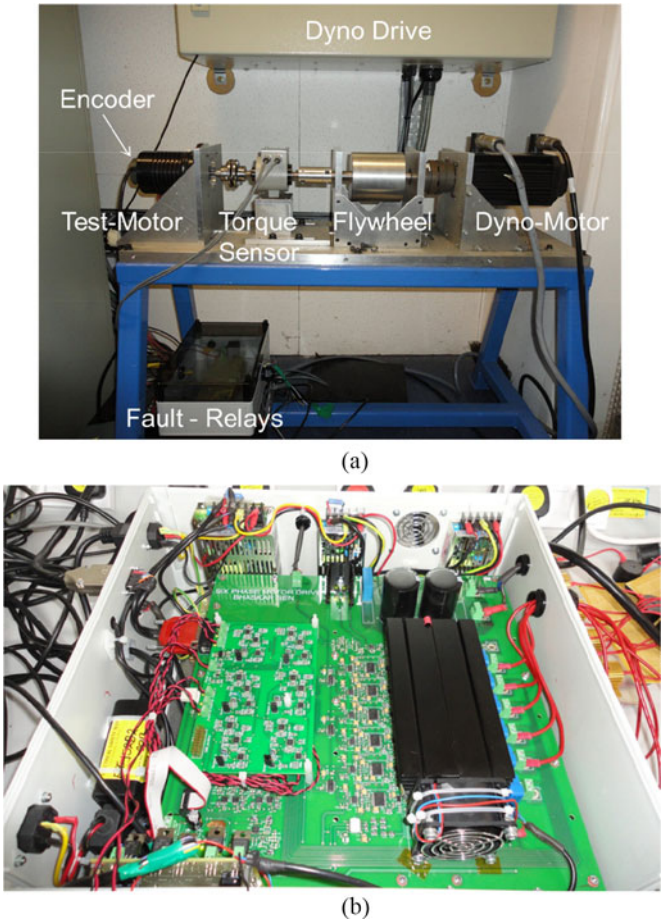

Fig. 16. (a) Dynamometer setup with test machine and fault relays and (b) five-phase inverter board.

loop is equal to $H(z)$, given as follows:

$$\frac{V(z)}{U(z)} = \frac{K_\infty}{1+\left(H(z)^{-1}-K_\infty^{-1}\right)K_\infty} = H(z). \qquad (20)$$

Since the term in the forward path of the controller is only a proportional gain and all the states of the controller (present in the feedback path) are driven only by the actual (saturated) values, windup does not occur [34].

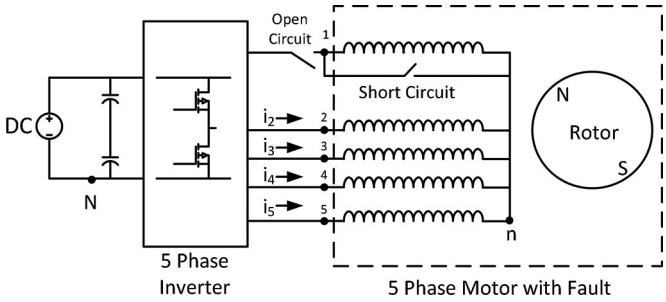

Fig. 17. Simplified schematic of the test setup.

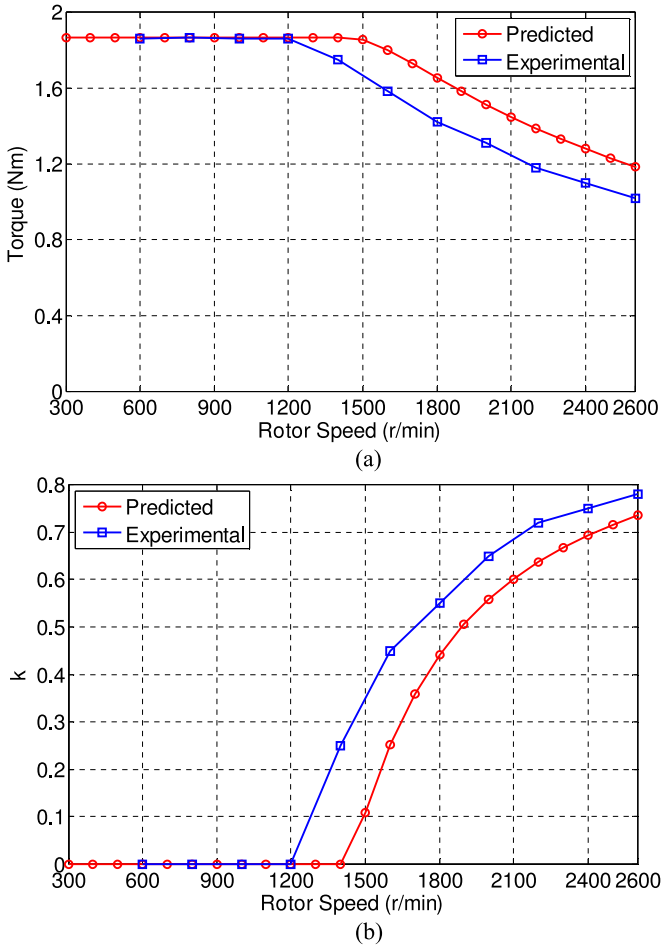

Fig. 18. (a) Torque–speed and (b) k-speed plots for healthy operation.

IV. Zero-Sequence Voltage Injection

By employing the proposed resonant controller, the current in each phase is controlled separately. The PWM signals for each inverter leg are also generated separately from the controller command voltage for each phase. To boost inverter output voltages, zero-sequence voltage is injected into the modulator inputs [39], as shown in Fig. 10.

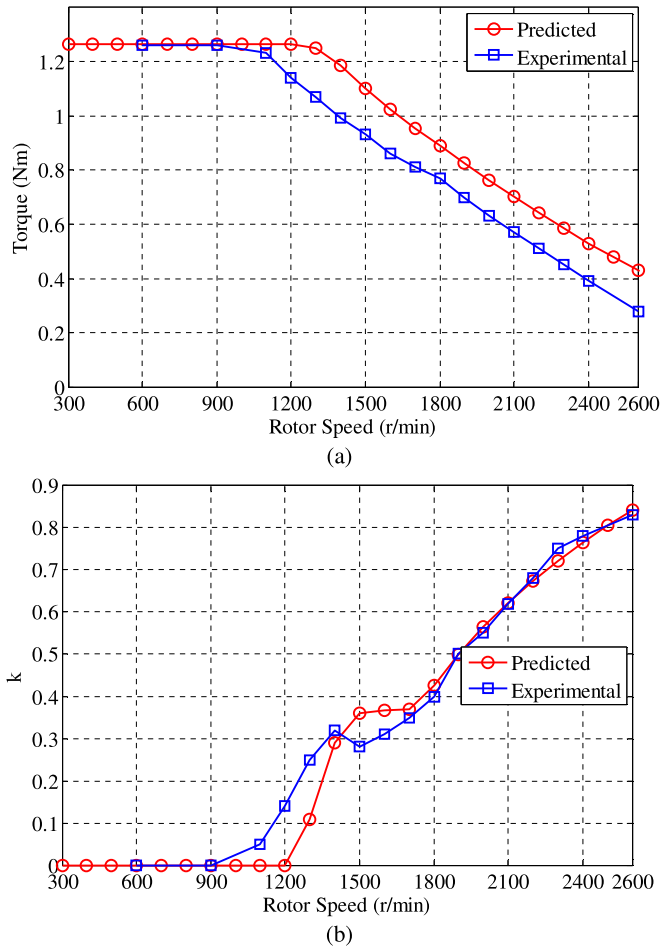

Fig. 19. (a) Torque–speed and (b) k-speed plots for phase-1 OC operation.

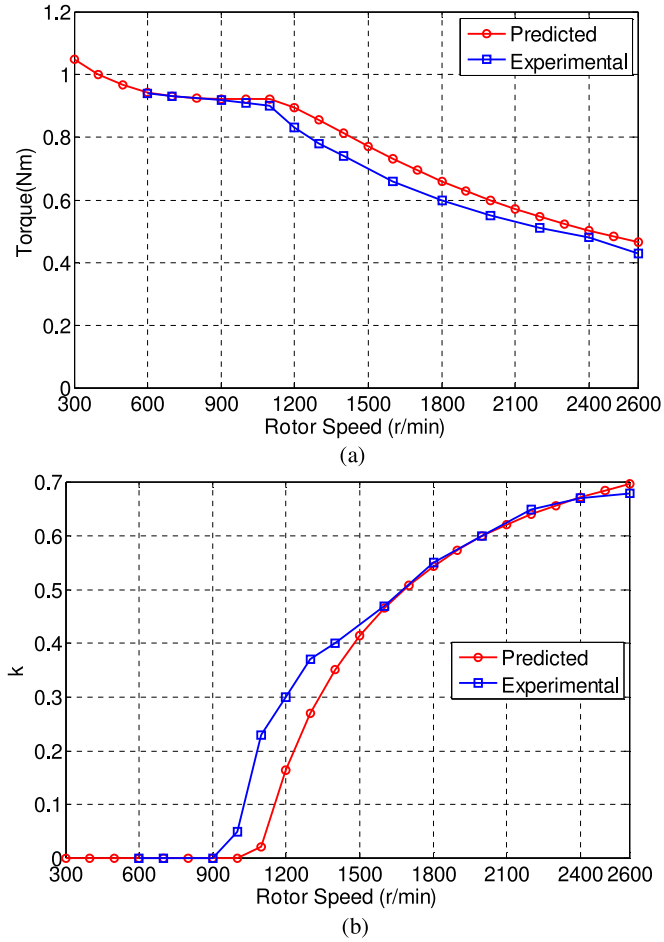

Fig. 20. (a) Torque–speed and (b) k-speed plots for phase-1 SC operation.

The injection of the zero-sequence voltage reduces the peak voltage command to the modulator without affecting the line-to-line voltage. By way of example, Fig. 11 compares sinusoidal modulation index command (M_i) in healthy conditions with the output of the voltage injection block. It can be seen that the output (M_i^*) is lower in magnitude (95.1%) than (M_i), and this can improve the torque–speed characteristic, especially in the field-weakening region.

Fig. 12 compares the torque–speed characteristics of the five-phase PM machine under healthy and fault conditions with and without the zero-sequence voltage injection. They are obtained by application of the OTC algorithm to generate phase current references under the voltage and current limits and assuming that tracking of these references are perfect. The weight factor for field weakening at a given speed is obtained by a search algorithm to maximize the torque under the voltage and current constraints. It can be observed that with the zero-sequence voltage injection, torque capability of the drive can be improved by around 9.18% in healthy case, around 22% in OC fault case, and around 30.8% in SC fault case at a speed of 1800 r/min.

Fig. 13 shows the final controller structure including voltage injection block, where $V_{\mathrm{j,unsat}}$ is the output of the jth phase proportional gain controller K_∞.

V. Field Weakening

On the basis of the analysis in Section II, the field weakening can be performed in the OTC scheme by changing the value of the field weakening constant k. The effect of changing k in (1) leads to an increase in the field weakening current at the same torque set point, so that the overall flux in the machine is reduced.

In [19], it was proposed that torque error be utilized for determining the amount of field weakening. This was performed since the control in [19] utilized hysteresis current controller and it is not possible to determine command voltages generated by the modulator. However, traditional field weakening control for PM machines utilizes voltage command to determine field weakening [40]. Fig. 14 shows the simulation result of varying k on peak current and voltages, at a fixed load torque $T_d = 0.71$ N·m and speed of 2000 r/min. It can be observed that as k is varied, peak current increases monotonically; however, peak voltage first decreases and then increases. Therefore, a key requirement for the k-update algorithm is to reduce the peak voltage and this is achieved using perturb and observe (P & O) algorithm. This is quite different from the traditional field weakening algorithm in healthy machines due to the unbalanced currents demanded by the OTC in fault condition. In this method, the sign of the last perturbation, i.e., change of k, and the sign of the last peak voltage change are used to determine the direction of next change

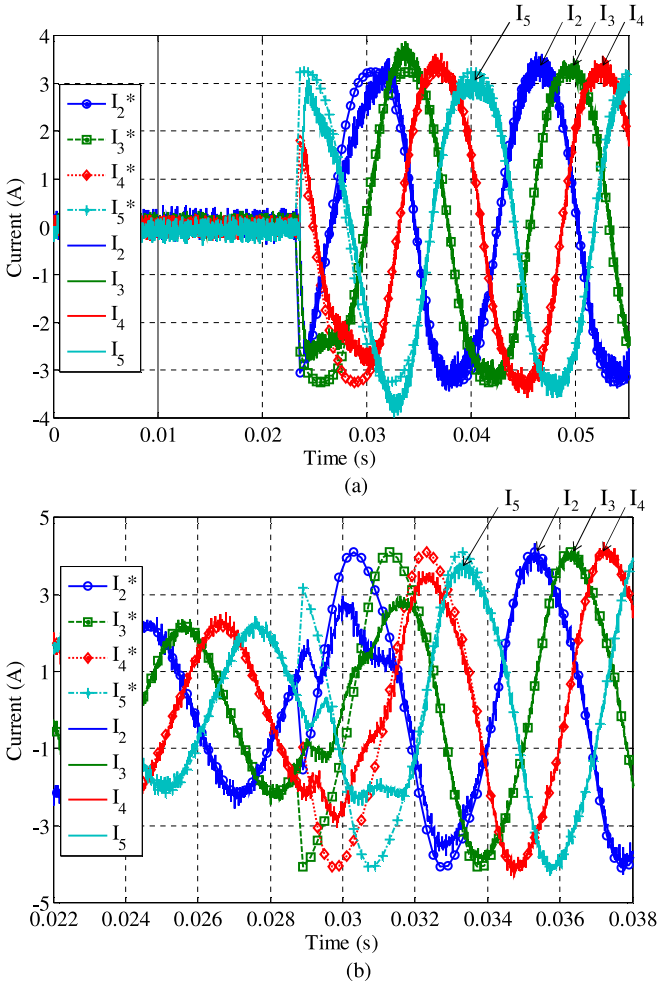

Fig. 21. Current response to step change in torque ($T_d = 0$ to 1 N·m) under healthy operation (a) at 0.023 s with $k = 0$ at 600 r/min (60 Hz) and (b) at 0.0287 s with $k = 0.3$ at 2000 r/min (200 Hz).

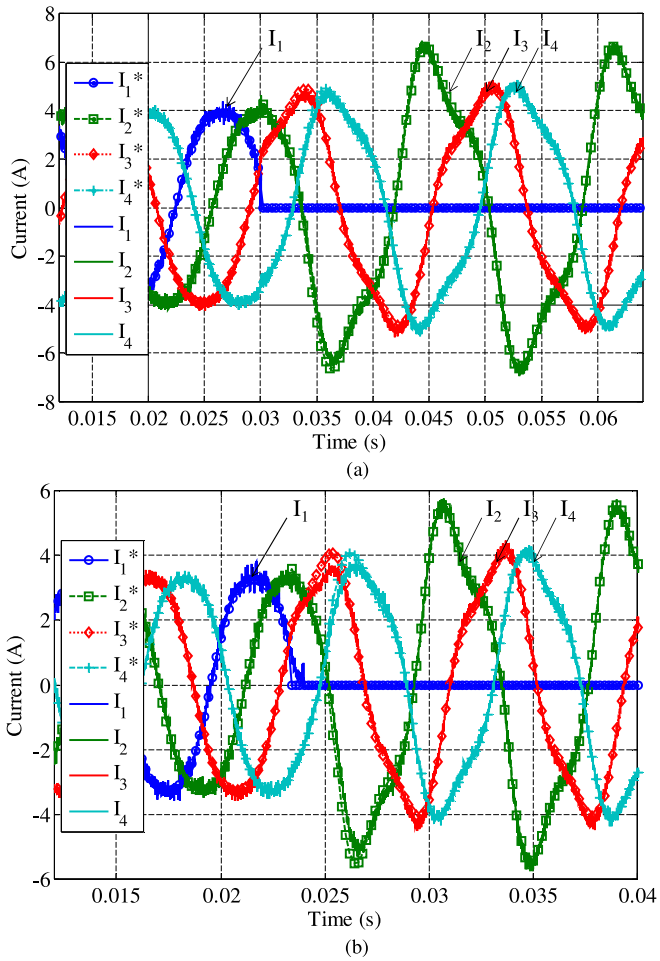

Fig. 22. Current response to transition from healthy to phase-1 OC (a) at 0.03 s with $T_d = 1.2$ N·m at 600 r/min (60 Hz) and (b) at 0.024 s with $T_d = 1$ N·m at 1200 r/min (120 Hz).

in value of *k*. If the peak voltage demand is less than $V_{\rm dc}/2$, *k* is reduced in order to reduce current demand, thereby reducing the copper losses. Due to the nonsinusoidal currents generated by the OTC under fault condition, voltage waveforms are also nonsinusoidal. Hence, peak voltage (V_{pk}) cannot be determined a priori; therefore, it is measured every electrical cycle by the controller. The field weakening algorithm is detailed in a flowchart shown in Fig. 15, where $V_{\rm th}$ is a threshold voltage used to reduce the effect of voltage noise on the algorithm. $V_{\rm th}$ is set at 1 V in this paper. The algorithm is evaluated every four electrical cycles denoted by *q* in order to allow the controller to settle after change in *k*. Although this field weakening controller will have a slower response compared to conventional field weakening control in healthy machines, it should be appreciated that under fault condition, the conventional field weakening controller cannot be used due to presence of unbalance and harmonic voltages.

VI. Experimental Results

To validate the developed fault-tolerant control strategy, a five-phase PM machine was designed and fabricated. The test-rig shown in Fig. 16(a) comprises of a Lenz dynamometer connected to the five-phase motor. An incremental encoder is used for rotor position feedback. A five-phase custom-built MOSFET inverter is used to control the motor as shown in Fig. 16(b). The inverter is controlled through a floating point TI DSP board (TMS320F28335 EzDSP). Commands to the DSP board are issued using either CAN interface via LabView or through the USB connection via the TI Code Composer studio. Fig. 17 shows the simplified schematic of the setup.

To validate the design, first steady-state torque–speed characteristics are obtained, by sweeping the T_d and *k* command until maximum torque is obtained without violating the voltage or current limit. Fig. 18 shows the predicted and measured torque–speed characteristics and variation of *k* with speed. The reduction in the measured torque is expected and is attributed to voltage drop in the devices, controller tracking error, and to variation in back-EMFs over a mechanical cycle due to tolerance on magnet properties and dimensions.

Figs. 19 and 20 show similar comparisons for the OC and SC fault in phase 1, respectively. To test the transient response of the current controller, step loading of 1 N·m (53% nominal load) is performed at 600 and 2000 r/min under healthy condition, as shown in Fig. 21. It can be observed that the controller settles

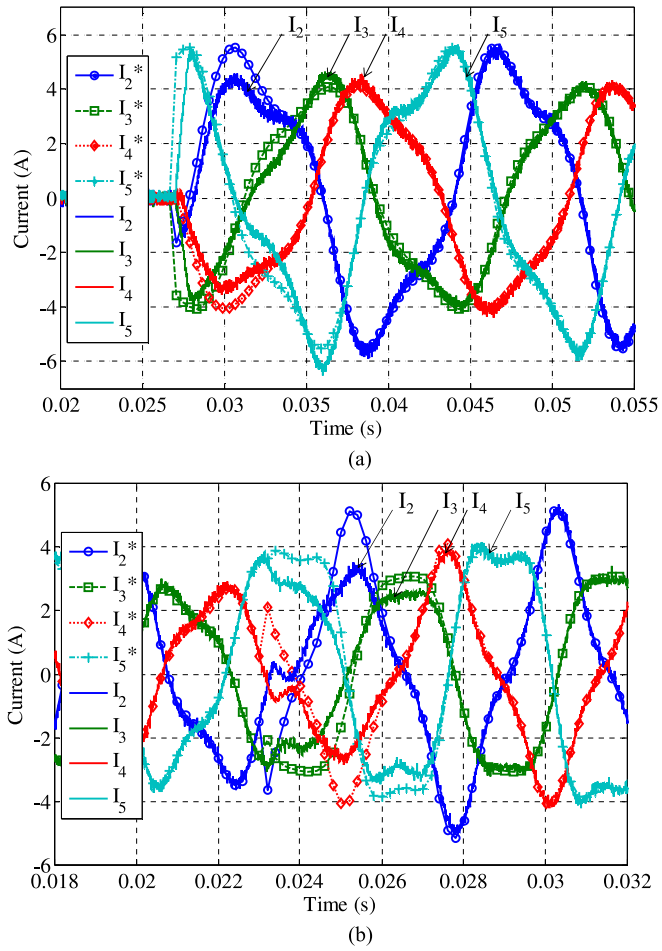

Fig. 23. Current response to step change in torque under phase-1 OC (a) $T_d = 0$ to 1 N·m at 0.027 s with $k = 0$ at 600 r/min and (b) $T_{\rm d} = 0$ to 0.6 N·m at 0.023 s with $k = 0.45$ at 2000 r/min.

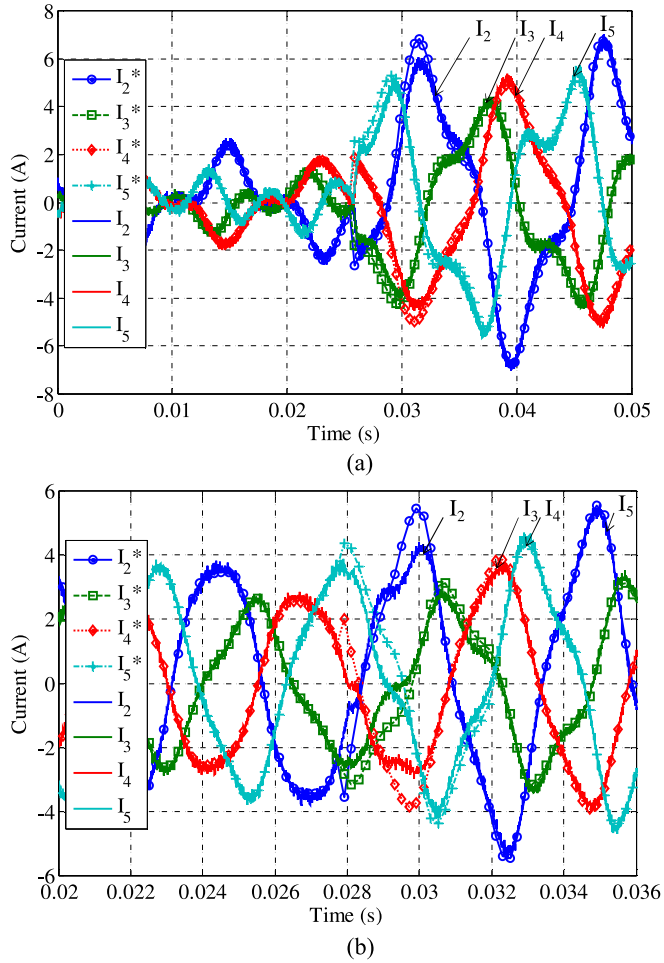

Fig. 24. Current response to step change in torque under phase-1 SC (a) $T_d = 0$ to 0.8 N·m at 0.025 s with $k = 0$ at 600 r/min; (b) $T_d = 0$ to 0. 45 N·m at 0.0278 s with $k = 0.45$ at 2000 r/min.

within 1.5 electrical cycles. Due to limitations of number of oscilloscope channels only four currents waveforms are shown.

To test the performance of the controller during transition from healthy to fault operating mode, an OC phase fault is initiated in phase 1 by opening phase-1 contactor at 0.03 s at 600 r/min and 0.024 s at 1200 r/min. The resultant current waveforms are shown in Fig. 22. It can be observed that the controller tracks new references within 1.5 electrical cycles.

Torque step responses under the OC are tested at 600 and 2000 r/min, and the results are shown in Fig. 23. It can be observed that the current settles in less than 1.5 electrical cycles. Similar tests are performed under the SC fault in phase 1 at 600 and 2000 r/min, and the current waveforms are shown in Fig. 24. It is to be noted that under the SC condition current references are not 0 even with $k = 0$ (no field weakening). This is expected since the OTC generates current references to cancel out the pulsating torque due to phase-1 SC. It is also worth mentioning that the speed regulation of the dynamometer used in the test setup is not ideal, and a step load change also causes a speed deviation of approximately 80 r/min, which causes the transient to exhibit slightly sluggish response compared to simulation.

Fig. 25 shows the response of field weakening controller at 2200 r/min with a torque step from 0.2 to 0.5 N·m. The

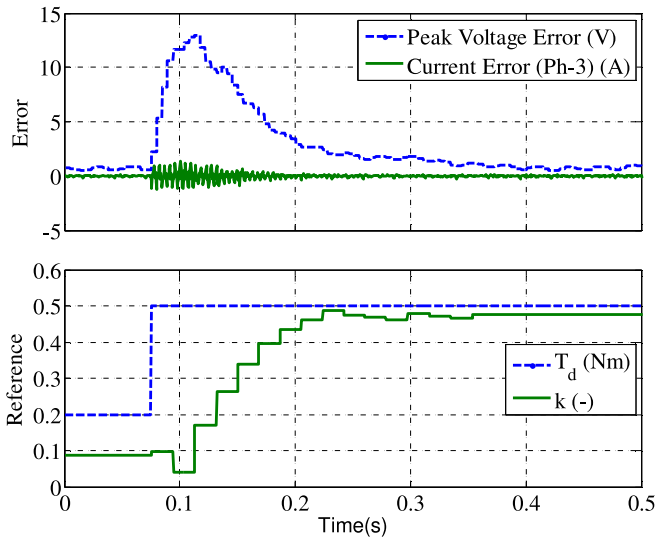

Fig. 25. Responses of voltage error, current tracking error, and the field weakening factor (k) to step change in torque (T_d) from 0.2 to 0.5 N·m under phase-1 OC at 2200 r/min.

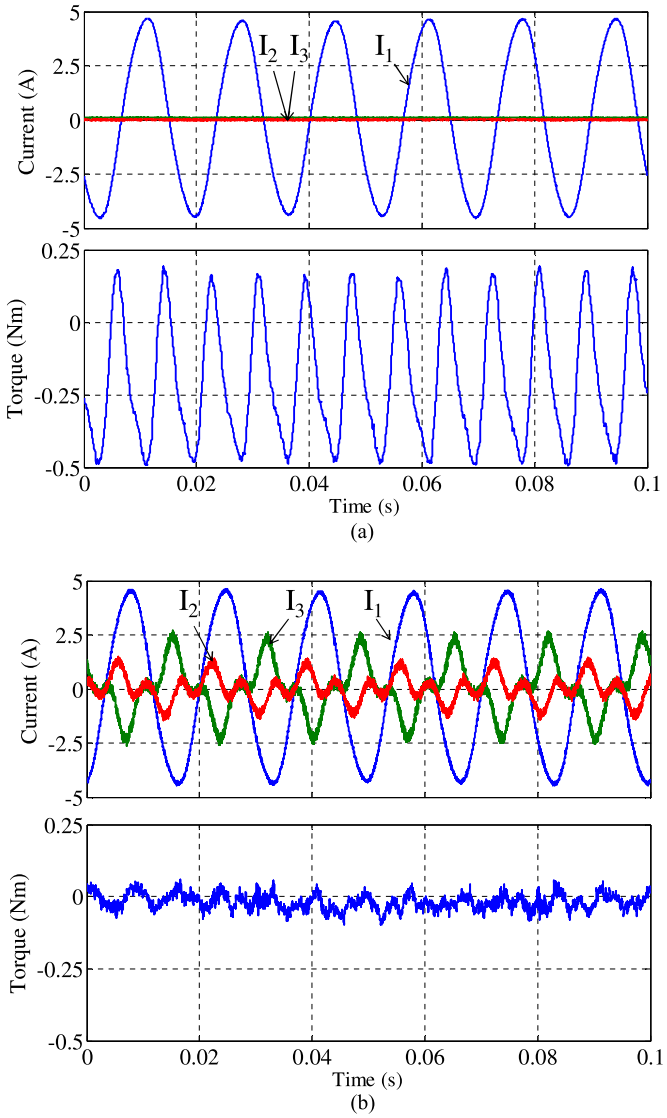

Fig. 26. Measured current and torque waveforms under SC (phase 1) at 600 r/min (a) without OTC control and (b) with OTC ($T_{\rm d} = 0$). I_1 is the SC current flowing in phase 1.

peak voltage error is the difference between the maximum peak voltage demand and the maximum inverter phase voltage $V_{\rm dc}/2$. It can be seen from the plot that the current tracking error is minimal after 0.2 s. It is to be noted that the torque step causes the speed of the machine to change, and this results is the variation of k to continue after 0.2 s.

The effect of the OTC on torque ripple reduction can be appreciated in measured torque in SC condition at $T_d = 0$ as shown in Fig. 26. It proves the efficacy of the OTC in achieving ripple torque reduction. Similar measurements under other operating conditions were also obtained but are not shown due to paper length limit.

VII. Conclusion

The paper has described and validated a novel current controller in natural stationary frame for fault-tolerant operation of polyphase machines. The unique contribution of the paper is a resonant control structure that allows pole–zero placements adapted to variable-speed operations. It also incorporates zero-sequence voltage injection and a suitable field weakening control to increase torque and speed operating range of a fault-tolerant permanent-magnet machine drive. It has been shown that the proposed control is capable of tracking unbalanced and nonsinusoidal current references over a wide speed range, including field weakening. The proposed control operates under both healthy and fault conditions with minimum reconfiguration. The methods presented in this paper provide new insights into the design of stationary frame-resonant controls for variable-speed drives.

References

[1] J. W. Bennett, G. J. Atkinson, B. C. Mecrow, and D. J. Atkinson, "Fault-tolerant design considerations and control strategies for aerospace drives," *Ind. Electron. IEEE Trans.*, vol. 59, no. 5, pp. 2049–2058, May 2012.

[2] M. E. H. Benbouzid, D. Diallo, and M. Zeraoulia, "Advanced fault-tolerant control of induction-motor drives for EV/HEV traction applications: From conventional to modern and intelligent control techniques," *IEEE Trans. Veh. Technol.*, vol. 56, no. 2, pp. 519–528, Mar. 2007.

[3] T. G. Habetler and Y. Lee, "Current-based condition monitoring and fault tolerant operation for electric machines in automotive applications," in *Proc. Int. Conf. Elect. Machines Syst.*, 2007, pp. 2011–2016.

[4] E. Levi, "Multiphase electric machines for variable-speed applications," *Ind. Electron. IEEE Trans.*, vol. 55, no. 5, pp. 1893–1909, May 2008.

[5] T.-H. Liu, J.-R. Fu, and T. A. Lipo, "A strategy for improving reliability of field-oriented controlled induction motor drives," *IEEE Trans. Ind. Appl.*, vol. 29, no. 5, pp. 910–918, Sep. 1993.

[6] J.-R. Fu and T. Lipo, "Disturbance-free operation of a multiphase current-regulated motor drive with an opened phase," *IEEE Trans. Ind. Appl.*, vol. 30, no. 5, pp. 1267–1274, Sep. 1994.

[7] H. A. Toliyat, "Analysis and simulation of five-phase variable-speed induction motor drives under asymmetrical connections," *IEEE Trans. Power Electron.*, vol. 13, no. 4, pp. 748–756, Jul. 1998.

[8] H. Xu, H. A. Toliyat, and L. J. Petersen, "Resilient current control of five-phase induction motor under asymmetrical fault conditions," in *Proc. 17th Annu. IEEE Appl. Power Electron. Conf. Expo.*, 2002, vol. 1, pp. 64–71.

[9] L. Parsa and H. A. Toliyat, "Five-phase permanent-magnet motor drives," *IEEE Trans. Ind. Appl.*, vol. 41, no. 1, pp. 30–37, Jan. 2005.

[10] N. Bianchi, S. Bolognani, and M. D. Pre, "Strategies for the fault-tolerant current control of a five-phase permanent-magnet motor," *Ind. Appl. IEEE Trans.,* vol. 43, no. 4, pp. 960–970, Aug. 2007.

[11] S. Dwari and L. Parsa, "Fault-tolerant control of five-phase permanent-magnet motors with trapezoidal back EMF," *IEEE Trans. Ind. Electron.*, vol. 58, no. 2, pp. 476–485, Feb. 2011.

[12] A. Mohammadpour and L. Parsa, "A unified fault-tolerant current control approach for five-phase pm motors with trapezoidal back EMF under different stator winding connections," *IEEE Trans. Power Electron.*, vol. 28, no. 7, pp. 3517 –3527, Jul. 2013.

[13] M. Salehifar, R. S. Arashloo, J. M. Moreno-Equilaz, V. Sala, and L. Romeral, "Fault detection and fault tolerant operation of a five phase pm motor drive using adaptive model identification approach," *IEEE J. Emerg. Sel. Top. Power Electron.*, vol. 2, no. 2, pp. 212–223, Jun. 2014.

[14] S. Dwari and L. Parsa, "Disturbance free operation of permanent magnet motor drives under short circuit faults using center-split winding," in *Proc. 42nd Conf. Rec. 2007 IEEE Ind. Appl. Conf. Annu. Meeting*, pp. 1329–1334.

[15] S. Dwari and L. Parsa, "Optimum fault-tolerant control of multiphase permanent magnet machines for open-circuit and short-circuit faults," in *Proc. 22nd Annu. IEEE Appl. Power Electron. Conf.*, 2007, pp. 1417–1422.

[16] S. Dwari, L. Parsa, and T. A. Lipo, "Optimum control of a five-phase integrated modular permanent magnet motor under normal and open-circuit fault conditions," in *Proc. IEEE Power Electron. Spec. Conf.*, 2007, pp. 1639–1644.

[17] A. Mohammadpour and L. Parsa, "Post-fault control technique for multiphase PM motor drives under short-circuit faults," in *Proc. 2013 28th Annu. IEEE Appl. Power Electron. Conf. Expo.*, pp. 817–822.
[18] A. Mohammadpour, S. Mishra, and L. Parsa, "Fault-tolerant operation of multiphase permanent-magnet machines using iterative learning control," *IEEE J. Emerg. Sel. Top. Power Electron.*, vol. 2, no. 2, pp. 201–211, Jun. 2014.
[19] Z. Sun, J. Wang, G. W. Jewell, and D. Howe, "Enhanced optimal torque control of fault-tolerant PM machine under flux-weakening operation," *IEEE Trans. Ind. Electron.*, vol. 57, no. 1, pp. 344–353, Jan. 2010.
[20] H.-M. Ryu, J.-W. Kim, and S.-K. Sul, "Synchronous-frame current control of multiphase synchronous motor under asymmetric fault condition due to open phases," *IEEE Trans. Ind. Appl.*, vol. 42, no. 4, pp. 1062–1070, Aug. 2006.
[21] F. Baudart, B. Dehez, E. Matagne, D. Telteu-Nedelcu, P. Alexandre, and F. Labrique, "Torque control strategy of polyphase permanent-magnet synchronous machines with minimal controller reconfiguration under open-circuit fault of one phase," *IEEE Trans. Ind. Electron.*, vol. 59, no. 6, pp. 2632–2644, Jun. 2012.
[22] H. S. Che, M. J. Duran, E. Levi, M. Jones, W.-P. Hew, and N. Abd Rahim, "Postfault operation of an asymmetrical six-phase induction machine with single and two isolated neutral points," *IEEE Trans. Power Electron.*, vol. 29, no. 10, pp. 5406–5416, Oct. 2014.
[23] X. Yuan, W. Merk, H. Stemmler, and J. Allmeling, "Stationary-frame generalized integrators for current control of active power filters with zero steady-state error for current harmonics of concern under unbalanced and distorted operating conditions," *IEEE Trans. Ind. Appl.*, vol. 38, no. 2, pp. 523–532, Apr. 2002.
[24] D. N. Zmood and D. G. Holmes, "Stationary frame current regulation of PWM inverters with zero steady-state error," *IEEE Trans. Power Electron.*, vol. 18, no. 3, pp. 814 – 822, May 2003.
[25] C. Lascu, L. Asiminoaei, I. Boldea, and F. Blaabjerg, "High performance current controller for selective harmonic compensation in active power filters," *IEEE Trans. Power Electron.*, vol. 22, no. 5, pp. 1826 –1835, Sep. 2007.
[26] A. Yepes, A. Vidal, F. D. Freijedo, J. Malvar, O. Lopez, and J. Doval-Gandoy, "Transient response evaluation of resonant controllers for AC drives," in *Proc. 2012 IEEE Energy Convers. Congr. Expo.*, pp. 471–478.
[27] S. Richter and R. W. De Doncker, "Digital proportional-resonant (PR) control with anti-windup applied to a voltage-source inverter," in *Proc. 14th Eur. Conf. Power Electron. Appl.,* 2011, pp. 1–10.
[28] B. P. McGrath, S. G. Parker, and D. G. Holmes, "High-performance current regulation for low-pulse-ratio inverters," *IEEE Trans. Ind. Appl.*, vol. 49, no. 1, pp. 149–158, Feb. 2013.
[29] K. Atallah, J. Wang, and D. Howe, "Torque-ripple minimization in modular permanent-magnet brushless machines," *IEEE Trans. Ind. Appl.*, vol. 39, no. 6, pp. 1689–1695, Dec. 2003.
[30] Z. Sun, J. Wang, D. Howe, and G. Jewell, "Analytical prediction of the short-circuit current in fault-tolerant permanent-magnet machines," *IEEE Trans. Ind. Electron.*, vol. 55, no. 12, pp. 4210 –4217, Dec. 2008.
[31] H.-M. Ryu, J.-H. Kim, and S.-K. Sul, "Analysis of multiphase space vector pulse-width modulation based on multiple d-q spaces concept," *IEEE Trans. Power Electron.*, vol. 20, no. 6, pp. 1364–1371, Nov. 2005.
[32] A. Tani, M. Mengoni, L. Zarri, G. Serra, and D. Casadei, "Control of multiphase induction motors with an odd number of phases under open-circuit phase faults," *IEEE Trans. Power Electron.*, vol. 27, no. 2, pp. 565–577, Feb. 2012.
[33] R. I. Bojoi, G. Griva, V. Bostan, M. Guerriero, F. Farina, and F. Profumo, "Current control strategy for power conditioners using sinusoidal signal integrators in synchronous reference frame," *IEEE Trans. Power Electron.*, vol. 20, no. 6, pp. 1402–1412, 2005.
[34] G. C. Goodwin, S. F. Graebe, and M. E. Salgado, *Control System Design*. Upper Saddle River, NJ, USA: Prentice Hall, 2001.
[35] A. G. Yepes, F. D. Freijedo, J. Doval-Gandoy, O. López, J. Malvar, and P. Fernandez-Comesaña, "Effects of discretization methods on the performance of resonant controllers," *IEEE Trans. Power Electron.*, vol. 25, no. 7, pp. 1692–1712, Jul. 2010.
[36] A. G. Yepes, F. D. Freijedo, O. Lopez, and J. Doval-Gandoy, "Analysis and design of resonant current controllers for voltage-source converters by means of Nyquist diagrams and sensitivity function," *IEEE Trans. Ind. Electron.*, vol. 58, no. 11, pp. 5231–5250, Nov. 2011.
[37] K. J. Astrom and T. Hagglund, *PID Controllers: Theory, Design and Tuning, 2nd Revised ed*. Research Triangle Park, NC, USA: ISA, 1995.
[38] *MATLAB Version 7.10.0*. Natick, MA, USA: MathWorks Inc., 2010.
[39] A. Iqbal and S. Moinuddin, "Comprehensive relationship between carrier-based PWM and space vector PWM in a five-phase VSI," *IEEE Trans. Power Electron.*, vol. 24, no. 10, pp. 2379–2390, Oct. 2009.
[40] T.-S. Kwon and S.-K. Sul, "Novel antiwindup of a current regulator of a surface-mounted permanent-magnet motor for flux-weakening control," *IEEE Trans. Ind. Appl.*, vol. 42, no. 5, pp. 1293–1300, Oct. 2006.

Bhaskar Sen (S'11) received the B.E. degree from Delhi College of Engineering, Delhi, India, in 2003, and the M.Tech. degree from Indian Institute of Technology, Kanpur, India, in 2006. He is currently working toward the Ph.D. degree from the University of Sheffield, Sheffield, U.K.

From 2006 to 2011, he was with GE Global Research, Bangalore, India. His current research interests include electrical machine fault modeling, machine fault detection, and fault-tolerant drives.

Jiabin Wang (S'94–M'96–SM'03) received the B.Eng. and M.Eng. degrees from Jiangsu University of Science and Technology, Zhengjiang, China, in 1982 and 1986, respectively, and the Ph.D. degree from the University of East London, London, U.K., in 1996, all in electrical and electronic engineering.

He is currently a Professor in Electrical Engineering at the University of Sheffield, Sheffield, U.K. From 1986 to 1991, he was with the Department of Electrical Engineering, Jiangsu University of Science and Technology, where he was appointed a Lecturer in 1987 and an Associated Professor in 1990. He was a Postdoctoral Research Associate at the University of Sheffield, from 1996 to 1997, and a Senior Lecturer at the University of East London from 1998 to 2001. His current research interests include motion control and electromechanical energy conversion devices, electric drives for applications in automotive, renewable energy, household appliances and aerospace sectors.

Dr. Wang is a Fellow of the Institute of Engineering and Technology, U.K.